Available online at www.sciencedirect.com
SCIENCE DIRECT
Journal of Solid State Chemistry 179 (2006) 1394–1400
JOURNAL OF SOLID STATE CHEMISTRY
www.elsevier.com/locate/jssc

Transport, magnetic, internal friction, and Young's modulus in the Y-doped manganites $La_{0.9-x}Y_xTe_{0.1}MnO_3$

G.H. Zheng, Y.P. Sun*, X.B. Zhu, W.H. Song

Key Laboratory of Materials Physics, Institute of Solid State Physics, Chinese Academy of Sciences, Hefei 230031, PR China

Received 6 November 2005; received in revised form 21 January 2006; accepted 29 January 2006
Available online 6 March 2006

Abstract

The resistivity, magnetization, internal friction, and Young's modulus for the polycrystalline samples $La_{0.9-x}Y_xTe_{0.1}MnO_3$ ($x = 0$, 0.05, 0.10 and 0.15) have been investigated. All samples have rhombohedral crystallographic structure with the space group $R\bar{3}C$. The Curie temperature T_C of the studied samples decreases with increasing Y-doping level. For the samples with $x = 0, 0.05$ and 0.10, the temperature dependence of the resistivity $\rho(T)$ exhibits two metal–insulator transitions (MIT) at T_{p1} (which is close to its Curie temperature T_C) and T_{p2} (which is below T_{p1}). When the doping level to 0.15, these two MIT temperatures are suppressed and an upturn at low temperatures below T^* is observed from the $\rho(T)$ curve. A change of Young's modulus E is observed in the vicinity of T_C accompanied by a broad peak of the internal friction Q^{-1} for all studied samples. The values of the relative Young's modulus ΔE increase with increasing Y-doping level at the low temperatures. These results are discussed in terms of the local Jahn–Teller (JT) distortion by the substitution of smaller Y^{3+} ions for larger La^{3+} ions and the increased bending of the Mn–O–Mn bond with decreasing the average ionic radius of the A-site element $\langle r_A \rangle$ and the tolerance factor t, resulting in the narrowing of the bandwidth, the decrease of the mobility of e_g electrons and the weakening of double-exchange (DE) interaction.

Keywords: A. Colossal magnetoresistance; D. Electrical transport; E. Strain

1. Introduction

Perovskite manganites $R_{1-x}A_xMnO_3$ (R = trivalent rare-earth ions such as La, Sm or Pr, A = divalent alkaline-earth ions such as Ca, Sr or Ba) have attracted enormous attention due to their fascinating negative colossal magnetoresistance (CMR) effect and potential technological applications for various functional devices. However, most of the previous studies are focused on hole-doped compounds with a mixed-valence state of Mn^{3+} and Mn^{4+}. Electron-doped compounds in which R were substituted by tetravalent ion such as Ce^{4+}, Te^{4+} and Zr^{4+}, etc., have been reported by some research groups [1–5]. These studies indicate that CMR behavior could occur in the system of a mixed-valence of Mn^{2+} and Mn^{3+}. However, only the paper [5] deals with the study of the structural, magnetic, and transport properties in the Pr-doped manganites $La_{0.9-x}Pr_xTe_{0.1}MnO_3$ ($0 \leqslant x \leqslant 0.9$).

It is well known that for the hole-doped manganites, the double-exchange (DE) interaction is considered as the main mechanism controlling both magnetic and transport properties [6]. However, there are some puzzling phenomena such as the magnitude of resistivity and the magnitude of CMR, which are not well understood. In order to explain the CMR effect quantitatively, electron–phonon coupling due directly to the dynamic Jahn–Teller (JT)-type distortion of the oxygen octahedral around Mn^{3+}, which is argued by Millis et al. [7,8], is believed to play a key role in the magnanites. For instance, near T_C, dramatic changes are observed in the lattice degree of freedom, the shift of phonon frequency, the anomalous lattice expansion and the anomalous sound velocity hardening, in which all reflect the closely relation between the lattice, and the electronic and magnetic properties [9–12]. Additional mechanisms such as the average ionic size of cations (R, A) [13,14], the size mismatch between R and A cations

*Corresponding author. Fax: +86 551 559 1434.
E-mail address: ghzheng@issp.ac.cn (G.H. Zheng).

0022-4596/$ - see front matter © 2006 Published by Elsevier Inc.
doi:10.1016/j.jssc.2006.01.068

or atomic disorder [15] also contributes to the physical properties of this system. The study of Hwang et al. [13] on $(La_{1-x}R_x)_{0.7}Ca_{0.3}MnO_3$ reveals that the T_C and the conductivity decrease when some La^{3+} is replaced by Pr^{3+} or Y^{3+}, in other words, the magnetic and transport properties of the system are a strong function of average A size ionic radius, $\langle r_A \rangle$. Based on these results, they have concluded that the electronic and magnetic state are highly relevant to a geometrical index called the Goldsmith tolerance factor t, which decides the crystallographic distortions from the cubic ($t = 1$) perovskite structure. The Goldsmith tolerance factor describes the stability of the perovskite structure and is defined as, $t = (r_A + r_O)/\sqrt{2}(r_B + r_O)$ where r_i ($i = A$, B, or O) represents the average ionic size of each element. With decreasing t, the Mn–O–Mn bond angle, to which the transfer integral is related and which describes the electron hopping between Mn^{3+} and Mn^{4+}, decreases. In addition, phase separation theory has been proposed to account for the CMR effect [16–18].

Y-doping in the hole-doped manganites $La_{0.60}Y_{0.07}Ca_{0.33}MnO_3$ [19] has aroused great interest due to the 'colossal' negative magnetoresistance (MR) $\approx -10{,}000\%$ with $T_C = 160$ K, in which the authors claim that the drop in T_C and the rise in the MR is related to the diminution of the unit cell due to the substitution of a smaller ion Y for La. Further studies of MR on this sample [20] at high external pressures have shown that the decrease in the unit cell produces the opposite effect: an increase in T_C and a decrease in MR. In addition, some researchers have found that there exists an anomaly in the linear thermal expansion at T_C that is suppressed by a magnetic field on the Y-doped compound [21]. In this paper, we have performed a detailed study on the physical properties of the electron-doped manganites $La_{0.9-x}Y_xTe_{0.1}MnO_3$ ($x = 0$, 0.05, 0.10 and 0.15), with fixed Mn^{2+}/Mn^{3+} ratio at 1/9, in terms of lattice, electric and magnetic properties, and internal friction and Young's modulus. And we will show that the average ionic radius of the A-site element affects strongly the microstructure, magnetic and transport properties in the electron-doped manganites $La_{0.9-x}Y_xTe_{0.1}MnO_3$ ($x = 0$, 0.05, 0.10 and 0.15).

2. Experimental details

Polycrystalline samples with nominal compositions $La_{0.9-x}Y_xTe_{0.1}MnO_3$ ($x = 0$, 0.05, 0.10 and 0.15, which are referred to as Y00, Y005, Y010 and Y015 below), were prepared by solid-state reaction method. Stoichiometric high-purity La_2O_3, Y_2O_3, TeO_2 and MnO_2 powders were mixed and ground, and then heated in air at 750 °C for 24 h. The powder obtained were ground, pressed into pellets and bars, and sintered at 1100 °C for 24 h with three intermediate grinding, and finally, the furnace was cooled down to room temperature. The structure and lattice constant were determined by powder X-ray diffraction (XRD) using Cu$K\alpha$ radiation at room temperature. The resistance as a function of temperature was measured by the standard four-probe method from 5 to 350 K under the magnetic fields of 0 and 5 T with a quantum design physical property measurement system (PPMS) ($2\,K \leqslant T \leqslant 400$ K, $0 \leqslant H \leqslant 9$ T). The magnetic measurements were carried out with a quantum design superconducting quantum interference device (SQUID) MPMS system ($5 \leqslant T \leqslant 400$ K, $0 \leqslant H \leqslant 5$ T). $Q^{-1}(T)$ and $E(T)$ were measured by the free decay method of a resonant bar in acoustic frequency range with magnitude of kHz and in the temperature range 80–370 K using warming mode in a helium gas environment at the rate of 0.3 K/min under zero applied magnetic field. The samples were excited electromagnetically in the fundamental free flexural modes. The internal friction Q^{-1} is defined as follows [22]:

$$Q^{-1} = \frac{1}{n} \ln\left(\frac{A_0}{A_n}\right), \tag{1}$$

where n is the number of the vibration cycles, while the amplitude attenuates from A_0 to A_n.

The Young's modulus E is given by

$$E = \frac{4\pi^2 s d l^4}{m^4 I} f^2, \tag{2}$$

where f is the resonant frequency, s the cross-sectional area, d the density, l the length, I the moment of inertia of the sample and m is 4.730 for the vibrating mode in the fundamental mode, in which the sample is suspended at two points whose span is 0.224 l from two free ends of the sample. Based on Eq. (2), E is proportional to the square of the resonant frequency, i.e., $E \propto f^2$. Therefore, we substitute f^2 for the Young's modulus E.

3. Results

3.1. X-ray diffraction

Fig. 1(a) show the XRD pattern of $La_{0.9-x}Y_xTe_{0.1}MnO_3$ ($x = 0$, 0.05, 0.10 and 0.15) samples. It can found that all samples are single phase with no detectable secondary phases. XRD patterns for all samples can be indexed by rhombohedral lattice with the space group $R\bar{3}C$, and we present experimental and calculated XRD patterns for the sample with $x = 0.15$ in Fig. 1(b). It can be seen that the fitting between the experimental spectra and calculated values is relatively good. The structural parameters are refined by the standard Rietveld technique and the fitting between the experimental spectra and the calculated values are shown in Table 1.

The Mn–O–Mn bond angle decreases with increasing the doping level x, whereas the Mn–O bond length increases which displays the inverse correlation to the variation in the Mn–O–Mn bond angle. It is well known that there are two possible origins of the lattice distortion of the perovskite structures: one is the deformation of the MnO_6 octahedra originating from the JT effect which is decided by the concentration of Mn^{3+} ions, and the other is the

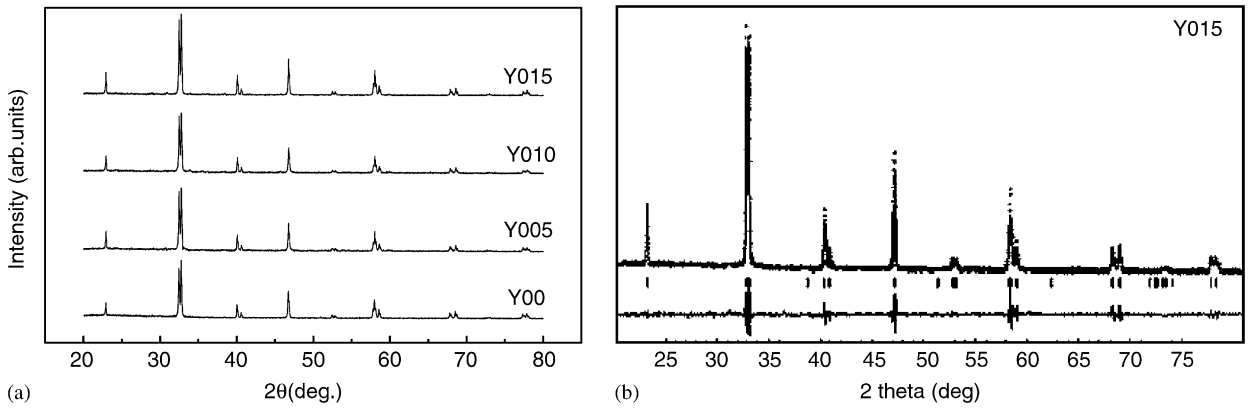

Fig. 1. (a) XRD patterns of the compound $La_{0.9-x}Y_xTe_{0.1}MnO_3$ ($x = 0$, 0.05, 0.10, 0.15). (b) The experimental and calculated XRD patterns of the compound Y015. Crosses indicate the experimental data and the calculated data is continuous line overlapping them. The lowest curve shows the difference between experimental and calculated patterns. The vertical bars indicated the expected reflection positions.

Table 1
Refined structural parameters of $La_{0.9-x}Y_xTe_{0.1}MnO_3$ ($x = 0$, 0.05, 0.10 and 0.15) at room temperature

Parameter	Y00	Y005	Y010	Y015
a (Å)	5.4761(35)	5.4855(20)	5.4866(18)	5.4881(21)
c (Å)	13.228(12)	13.2658(32)	13.2664(13)	13.2680(27)
Mn–O (Å)	1.8401	1.8502	1.8795	1.8825
Mn–O–Mn (Å)	167.09	166.71	164.58	161.39
R_p (%)	8.32	9.55	8.55	7.23

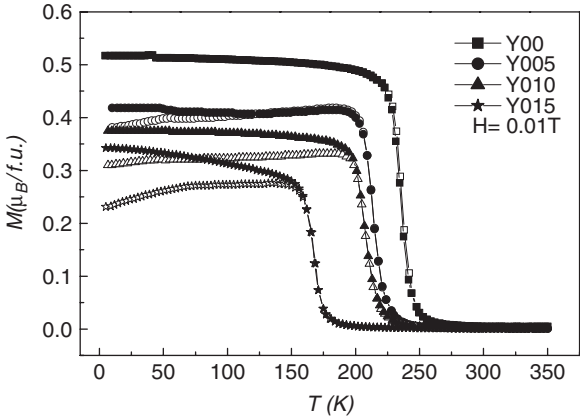

Fig. 2. Magnetization as a function of temperature $M(T)$ for $La_{0.9-x}Y_xTe_{0.1}MnO_3$ ($x = 0$, 0.05, 0.10 and 0.15) measured at $H = 0.01$ T.

average ionic radius of the A-site element $\langle r_A \rangle$. In the present samples, the concentration of Mn^{3+} is fixed and the lattice distortion is ascribed to the variation of the average A-site radius $\langle r_A \rangle$, induced by the substitution of smaller Y^{3+} for larger La^{3+} ions.

3.2. Magnetic properties

Temperature dependence of the magnetization $M(T)$ presented in Fig. 2 was measured in both zero-field-cooling (ZFC) and field-cooling (FC) modes at an applied magnetic field of 0.01 T. All samples undergo the paramagnetic (PM)–ferromagnetic (FM) phase transition. The Curie temperature T_C (defined as the one corresponding to the peak of dM/dT vs. T curve) are 238, 212, 208, and 168 K for $x = 0$, 0.05, 0.10 and 0.15, respectively. Obviously, with increasing Y content, the PM–FM transition shifts to lower temperatures and the magnetization decreases. The phenomenon can be interpreted as the reduction of the Mn–O–Mn bond angle with decreasing the average A-site element $\langle r_A \rangle$ due to the partial substitution of smaller Y^{3+} ions for larger La^{3+} ions. The substitution causes the narrowing of the bandwidth and the decreasing of the mobility of e_g electrons resulting in the weakness of DE interaction. In addition, from Fig. 2, it can be seen that the ZFC curve does not coincide with the FC curve at low temperatures for the Y-doping samples. This discrepancy between ZFC and FC $M(T)$ curves is a characteristic of magnetic inhomogeneity. Generally, the magnetic inhomogeneity is considered as the competition between FM phase and antiferromagnetic (AFM) phase. With increasing the doping level x for the same doping element, the difference between FC and ZFC $M(T)$ curves becomes larger implying the increase of magnetic inhomogeneity with increasing the doping level x.

3.3. Electrical properties

Fig. 3 presents the temperature dependence of resistivity for all samples at $H = 0$ and 5 T fields in the temperature range of 5–350 K. The samples Y00, Y005 and Y010 exhibit two metal–insulator (M–I) transitions. The higher-temperature transition peak, denoted by T_{P1}, is 238 for Y00, 212 K for Y005 and 206 K for Y010, which is close to their Curie temperature T_C, 240 K for Y00, 212 K for Y005 and 208 K for Y010. The lower-temperature transition peak, denoted by T_{P2}, is 192 K for Y00, 172 K for Y005

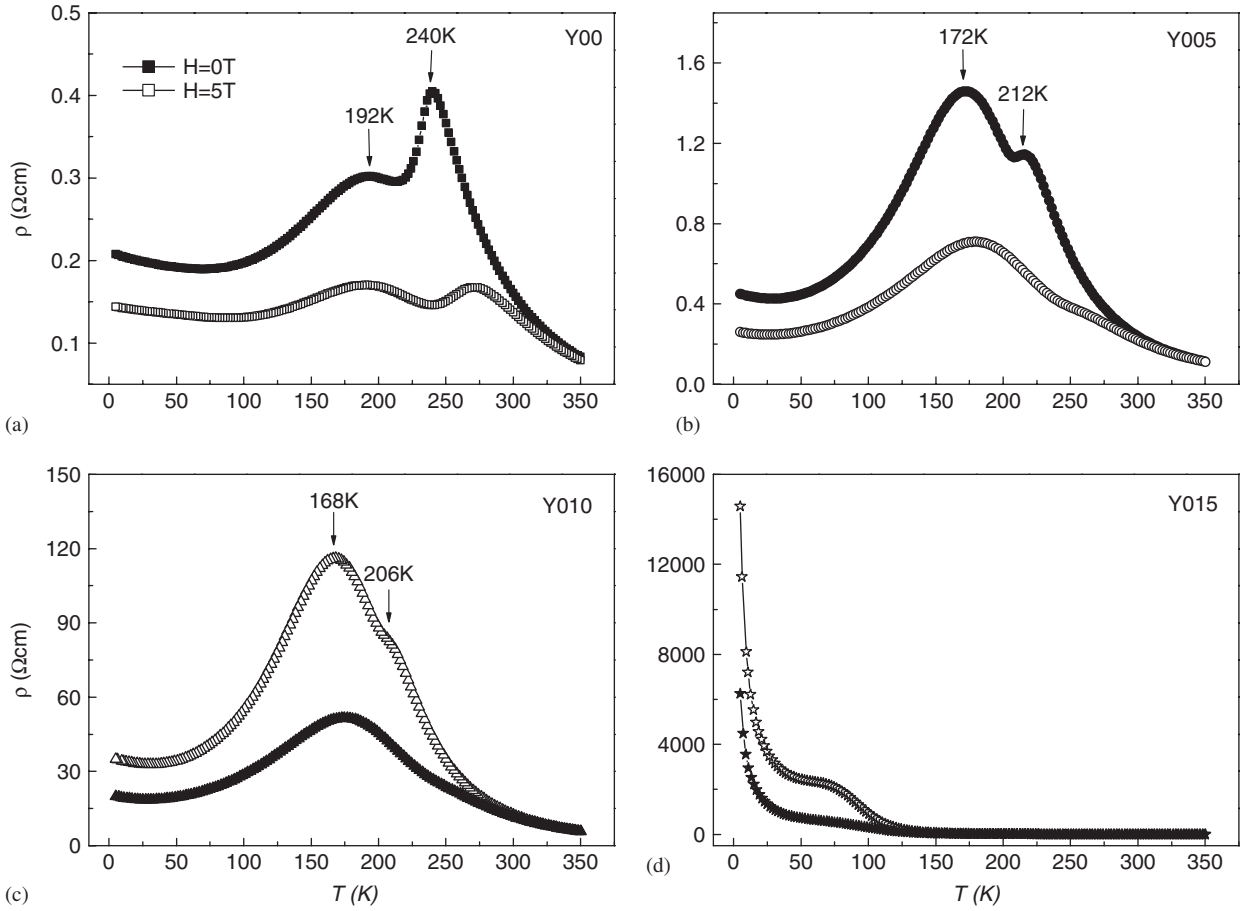

Fig. 3. The temperature dependence of the resistivity $\rho(T)$ for the samples $La_{0.9-x}Y_xTe_{0.1}MnO_3$ (a) $x = 0$, (b) $x = 0.05$, (c) $x = 0.10$ and (d) $x = 0.15$ at 0 and 5 T fields.

and 168 K for Y010, which is well below T_C, respectively. The phenomena with double-peak-type ρ-T behavior have also been observed in both alkaline-earth-metal-doped and alkali-metal-doped samples of $LaMnO_3$ [23–26]. When $x = 0.15$, the two MIT transitions are suppressed and an upturn at low temperatures below $T^*(= 45\,K)$ is observed. It is obvious that the resistivity increases with increasing Y-doping level. The phenomenon is usually explained according to decreased average ionic radius of the A-site element $\langle r_A \rangle$ with increasing doping level x, which reduces the FM coupling due to reduced band width of e_g electron.

It is very worth pointing out that T_{P1} and T_{P2} show the different response to the applied magnetic field. In addition, no MR peak (or bump) at T^* is observed for the Y015 sample. It is observed that the resistivity of the samples decreases, the T_{P2} move toward higher temperature and T_{P1} disappears under the applied magnetic field. And it leads to negative MR. The temperature dependence of the MR of the samples is presented in Fig. 4. Here the MR is defined as $MR = (\rho_0 - \rho_H)/\rho_0 \times 100(\%)$, where ρ_0 is the resistivity at zero field and ρ_H is the resistivity at $H = 5\,T$. With increasing the Y-doping level, the peak at T_{P1} becomes weak and the bump at T_{P2} becomes obvious, which is in accordance with the $\rho(T)$ behavior.

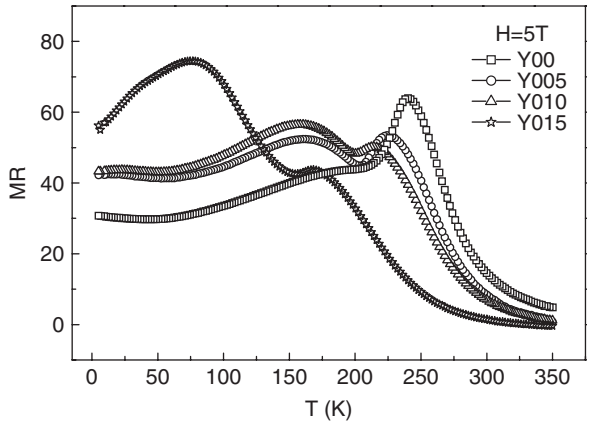

Fig. 4. The temperature dependence of the magnetoresistance (MR) ratio of $La_{0.9-x}Y_xTe_{0.1}MnO_3$ ($x = 0$, 0.05, 0.10 and 0.15) at $H = 5\,T$.

According to the DE model, in the homogeneous FM state, the electrons are mobile and the FM state and metallic state should accompany and facilitate each other. In contrast, the transport property of the studied samples

does not fully show metallic state below T_C. The FM order at low temperatures for the studied samples can be understood by the presence of FM clusters. On the one hand, based on the coexistence of FM clusters and AFM insulating phase in the low temperature region, we may suggest that the spatially inhomogeneous metallic and insulating areas coexist in the studied samples. When the system is transferred from PM to FM phase with the decrease of temperatures, the transport property of the samples does not fully show the metallic state because the FMM phases are disconnected for the existence of the FMI phases among them. For Y00, Y005 and Y010, with further decrease of temperature below T_C or under the applied magnetic field, the FMI region decreases and the metallic phases are connected in a percolative manner. However, for the Y015 sample, the percolative channel is blocked and the upturn of resistivity in the low temperature region appears. On the other hand, the $La_{0.9-x}Y_xTe_{0.1}MnO_3$ is a system with electric and magnetic disorder due to the substitution of smaller Y^{3+} for larger La^{3+} ions. This disorder may lead to electron localization and give rise to insulating region at low temperatures. And with increasing the doping level x, the insulating phase increases, even for the Y015 sample the resisitvity curve seems as insulating behavior.

3.4. Internal friction and Young's modulus

In order to understand the effect that the larger La is substituted by the smaller ionic size Y further, we measured the temperature dependence of Young's modulus E and internal friction Q^{-1} for all samples as shown in Fig. 5. The internal friction measuring technique has been proven to be particularly useful for probing systems undergoing magnetic and structural phase transitions [27–29].

As is well known, E is closely related to cohesive force among atoms and is proportional to the inverse of the static strain if the external force is kept in a constant. Therefore, the variation of E also actually reflects the information of the lattice variation. Comparing the large change of E and Q^{-1} in $La_{0.67}Ca_{0.33}MnO_3$ with orthorhombic *Pnma*, the variation of E and Q^{-1} in the samples $La_{0.9-x}Y_xTe_{0.1}MnO_3$ with the $R\bar{3}C$ space group is small, which can be ascribed to the structural difference. The orthorhombic structure with the space group *Pnma* allows three independent Mn–O bond lengths, and can therefore accommodate a static coherent distortion of the MnO_6 octahedra. The $R\bar{3}C$ space group enforces on average equal Mn–O bond lengths and prevents static coherent JT-type distortions of the MnO_6 octahedra. Recent neutron-diffraction experiments [30] have indicated that no obvious JT-type distortions exist in rhombohedral

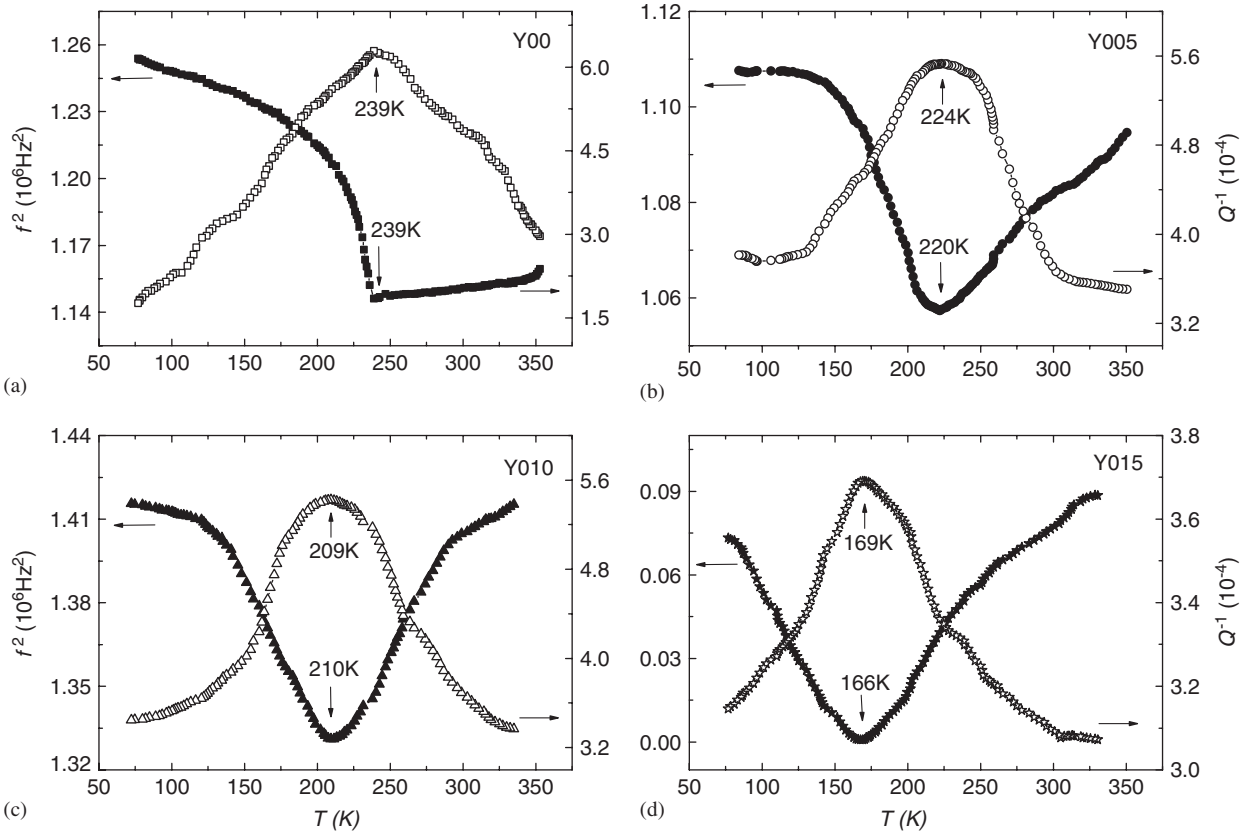

Fig. 5. The temperature dependence of internal friction Q^{-1} and Young's modulus E for the samples $La_{0.9-x}Y_xTe_{0.1}MnO_3$: (a) $x = 0$, (b) $x = 0.05$, (c) $x = 0.10$ and (d) $x = 0.15$.

$La_{0.67}Sr_{0.33}MnO_3$. However, Louca et al. [31] suggested that the local atomic structure significantly deviates from the average, and that the local JT distortion persists even when the crystallographic structure shows no JT distortion. Theoretically, Millis and co-workers [7,8] proposed a dynamical model with temporally (and spatially) fluctuating local JT distortions. So, in the case, we may suggest that E reflects the dynamic incoherent local JT distortion.

As shown in Fig. 5, near the FM transition T_C, E stiffening is observed for all samples below T_C with decreasing temperatures, and at the temperature above T_C, there is a softening as the transition is approached from higher temperatures. The temperature of the change of E is defined as T_E, and the value is 239, 220, 210 and 166 K for Y00, Y005, Y010 and Y015, respectively. The large change of E in the vicinity T_C actually means that there exist lattice distortions accompanied by PM–FM transition, which are driven by the JT effect due to Mn^{3+}. High-resolution neutron powder diffraction study indicates that the cell volume contracts at the Curie point accompanied by a remarkable decrease of the JT distortion MnO_6 octahedra in Ref. [32]. Microscopically, it is related to the spin and lattice coupling. In PM state, dynamic incoherent JT distortions lower the symmetry of the local MnO_6 octahedra thus there exists three independent Mn–O lengths. In FM state, the dynamic JT distortions decrease and the MnO_6 octahedra symmetry are improved. Accompanied by anomalous modulus, the internal friction Q^{-1} shows a broad peak in the vicinity of T_C for all samples. The Q^{-1} broad peak is suggested to originate from the change of magnetic entropy in the process of magnetic transition [33,34]. In other words, the magnetic entropy of the samples will have large loss when the samples undergo transition from magnetically disordered PM state to ordered FM one.

It is worth pointing out that the change of E and Q^{-1} occurs in the vicinity of T_{P1} (which is close to T_C) while no anomalous phenomena are observed in the vicinity of T_{P2} for Y00, Y005 and Y010. The resistivtity of the sample Y015 shows semiconducting behavior, which maybe ascribed to the large local distortions. Using the Hamiltonian of small polarons with a strong electron–phonon coupling interaction, Min et al. [35,36] have investigated the anomalous behaviors of sound velocity in CMR manganese oxides and they calculated a sound velocity hardening below the FM transition temperature. It means that carrier delocalization results in a weaker electron–phonon coupling, and this weakens the driving force for JT distortion from Mn^{3+}. This result demonstrates that there is a close correlation between charge and lattice. Hence, based on the above results, it can be deduced that there exists a strong correlation among lattice, spin and charge freedoms of degree.

In addition, we present the relative modulus as a function of temperature, where ΔE is defined as $\Delta E = (E - E_{min})/E_{min}$, for $La_{0.9-x}Y_xTe_{0.1}MnO_3$ series as shown in Fig. 6. One may find that there is a similar trend

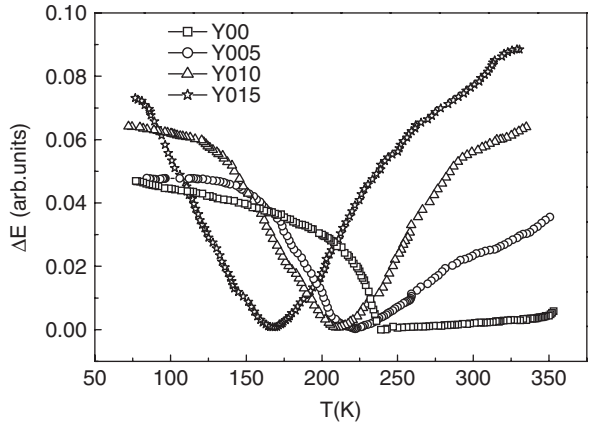

Fig. 6. The relative modulus vs. temperature for $La_{0.9-x}Y_xTe_{0.1}MnO_3$ ($x = 0$, 0.05, 0.10 and 0.15).

for all samples in quality, however, a large difference in quantity. The relative stiffening of the Young's modulus ΔE can be viewed as a scale of the magnitude of the JT distortion. So, the variation of ΔE with x, implies that the magnitude of the JT distortion and its associated effective strength of electron–lattice interaction strongly depend on the doping level x. According to Millis's calculation [8], the substitution of Y for La decreases the effective Mn d–d overlap and increases the electron–phonon interaction thus ΔE increases with an increasing Y doping level in the low-temperature region, which is accordance with the magnetic and electric transport for the studied samples. In addition, the result also implies the MnO_6 octahedra distortion is slighter for small ΔE values compared with that of the compound with orthorhombic *Pnma*.

4. Conclusions

Using magnetization, resistivity, Young's modulus and internal friction techniques, we have investigated the A-site (La-site) ionic size effects on polycrystalline samples $La_{0.9-x}Y_xTe_{0.1}MnO_3$ ($x = 0$, 0.05, 0.10 and 0.15). The substitution of smaller size Y at the La site shifts both the insulator–metal transition temperature and the Curie temperature to lower values accompanied with a subsequent increase in resistivity. For the samples with $x = 0$, 0.05 and 0.10, there exists two insulator–metal transitions. When $x = 0.15$, the two MIT transitions are suppressed and an upturn at low temperatures below $T^*(= 45\,K)$ is observed. Both the changes of Young's modulus E and internal friction Q^{-1} are observed in the vicinity of T_C for all samples that result from the change of microscopic structure at the transition temperature. The fact that the values of relative Young's modulus ΔE increase with increasing the doping level at low temperatures is attributed to the increase of the magnitude of JT distortion. These results indicate the presence of strong electron–phonon and spin–phonon coupling.

Acknowledgments

This work was supported by the National Key Research under contract No. 001CB610604 and the National Nature Science Foundation of China under contract Nos. 10474100, 10374033, and the Fundamental Bureau of the Chinese Academy of Sciences.

References

[1] J.M.D. Coey, M. Viret, S. von Molnár, Adv. Phys. 48 (1997) 167.
[2] T. Ohon, K. Chahara, Y. Kosona, Appl. Phys. Lett. 63 (1993) 1990.
[3] S. Jin, T.H. Tiefel, M. McCormack, R.A. Fastnacht, R. Ramesh, L.H. Chen, Science 264 (1994) 413.
[4] P. Mandal, S. Das, Phys. Rev. B 56 (1997) 15073.
[5] J. Yang, W.H. Song, Y.Q. Ma, R.L. Zhang, B.C. Zhao, Z.G. Sheng, G.H. Zheng, J.M. Dai, Y.P. Sun, Phys. Rev. B 70 (2004) 144421.
[6] C. Zener, Phys. Rev. 82 (1951) 403.
[7] A.J. Millis, P.B. Littlewood, B.I. Shraiman, Phys. Rev. Lett. 74 (1996) 5144.
[8] A.J. Millis, B.I. Shraiman, R. Mueller, Phys. Rev. Lett. 77 (1996) 175.
[9] M.R. Ibarra, P.A. Algarabel, C. Marquina, J. Blasco, J. García, Phys. Rev. Lett. 75 (1995) 3541.
[10] K.H. Kim, J.Y. Gu, H.S. Choi, G.W. Park, T.W. Noh, Phys. Rev. Lett 77 (1996) 1877.
[11] P. Dai, J.D. Zhang, H.A. Mook, S.H. Liou, P.A. Dowben, E.W. Plummer, Phys. Rev. B 54 (1996) R3694.
[12] A.P. Ramirez, P. Schiffer, S.-W. Cheong, C.H. Chen, W. Bao, T.T. Palstra, P.L. Gammel, D.J. Bishop, B. Zegarski, Phys. Rev. Lett. 76 (1996) 3188.
[13] H.Y. Hwang, S.-W. Cheong, P.G. Radaelli, M. Marezio, B. Batlogg, Phys. Rev. Lett. 75 (1995) 914.
[14] J. Blasco, J. García, J.M. de Tereas, M.R. Ibarra, P.A. Algarabel, C. Marquina, J. Phys.: Condens. Matter 8 (1996) 7427.
[15] L.M. Rodriguez-Martinez, J.P. Attfield, Phys. Rev. B 54 (1996) R15622.
[16] A. Moreo, S. Yunoki, E. Dagotto, Science 283 (1999) 2034.
[17] M. Fath, S. Freisem, A.A. Menovsky, Y. Tomiooka, J. Aarts, J.A. Mydosh, Science 285 (1995) 1540.
[18] E. Dagotto, T. Hotta, A. Moreo, Phys. Rep. 344 (2001) 1.
[19] S. Jin, H.M. O'Bryan, T.H. Tiefel, M. McComack, W.W. Rhodes, Appl. Phys. Lett. 66 (1995) 382.
[20] Z. Arnold, K. Kamenev, M.R. Ibarra, P.A. Algarabel, C. Marquina, J. Blasco, J. García, Appl. Phys. Lett. 67 (1995) 2875.
[21] M.R. Ibarra, P.A. Algarabel, C. Marquina, J. Blasco, J. García, Appl. Phys. Lett. 75 (1995) 541.
[22] J.J. Du, Y.P. Sun, J.Y. Jiang, F.C. Zeng, H.Q. Yin, Phys. Rev. B 41 (1990) 6679.
[23] S.L. Ye, W.H. Song, J.M. Dai, S.G. Wang, K.Y. Wang, C.L. Yuan, Y.P. Sun, J. Appl. Phys. 88 (2000) 5915.
[24] K. Sattler, J. Mühlbach, E. Recknagel, Phys. Rev. Lett. 45 (1980) 821.
[25] J.A. Cowen, B. Stolzman, R.S.A. Averback, H.J. Han, Appl. Phys. 61 (1987) 3317.
[26] S.L. Ye, W.H. Song, J.M. Dai, S.G. Wang, K.Y. Wang, C.L. Yuan, J.J. Du, Y.P. Sun, J. Fang, J.L. Chen, B.J. Gao, J. Appl. Phys. 90 (2000) 2943.
[27] G.J. Snyder, R. Hiskes, S. Dicarolis, M.R. Beasley, T.H. Geballe, Phys. Rev. B 53 (1998) 14103.
[28] Y.Q. Ma, W.H. Song, R.L. Zhang, J.M. Dai, J. Yang, J.J. Du, Y.P. Sun, Phys. Rev. B 69 (2004) 134404.
[29] C.F. Zhu, R.K. Zheng, J.R. Su, J. He, Appl. Phys. Lett. 74 (1999) 3504.
[30] P.G. Radaelli, M. Marezio, H.Y. Hwang, S.-W. Cheong, B. Batlogg, Phys. Rev. B 54 (1996) 8992.
[31] D. Louca, T. Egami, E.L. Brosha, H. Röder, A.R. Bishop, Phys. Rev. B 56 (1997) R8475.
[32] J.L. García-Muñoz, M. Suaaidi, J. Fontcuberta, J. Rodríguez-Carvajal, Phys. Rev. B 55 (1996) 34.
[33] K.B. Li, X.J. Li, C.S. Liu, Z.G. Zhu, J.J. Du, D.L. Hou, X.F. Nie, J.S. Zhu, Y.H. Zhang, Phys. Rev. B 56 (1997) 13662.
[34] F. Cordero, C. Castellano, R. Cantelli, M. Ferretti, Phys. Rev. B 65 (2002) 012403.
[35] B.I. Min, J.D. Lee, S.J. Youn, Magn. Magn. Mater. 181 (1998) 881.
[36] J.D. Lee, B.I. Min, Phys. Rev. B 55 (1997) 12454.